

Real time high accuracy phase contrast imaging with parallel acquisition speckle tracking

Zhe Hu(胡哲), Wen-Qiang Hua(滑文强), and Jie Wang(王劼)

Citation: Chin. Phys. B, 2021, 30 (**6**): 064201. DOI: 10.1088/1674-1056/abee08
Journal homepage: http://cpb.iphy.ac.cn; http://iopscience.iop.org/cpb

What follows is a list of articles you may be interested in

Handwritten digit recognition based on ghost imaging with deep learning

Xing He(何行), Sheng-Mei Zhao(赵生妹), and Le Wang(王乐)
Chin. Phys. B, 2021, 30 (**5**): 054201. DOI: 10.1088/1674-1056/abd2a5

Three-dimensional spatial multi-point uniform light focusing through scattering media based on feedback wavefront shaping

Fan Yang(杨帆), Yang Zhao(赵杨), Chengchao Xiang(向成超), Qi Feng(冯祺), and Yingchun Ding(丁迎春)
Chin. Phys. B, 2021, 30 (**4**): 044207. DOI: 10.1088/1674-1056/abe3e6

A scanning distortion correction method based on *X*- *Y* galvanometer Lidar system

Bao-Ling Qi(漆保凌), Chun-Hui Wang(王春晖), Dong-Bing Guo(郭东兵), and Bin Zhang(张斌)
Chin. Phys. B, 2021, 30 (**4**): 044206. DOI: 10.1088/1674-1056/abcf42

Incoherent digital holographic spectral imaging with high accuracy of image pixel registration

Feng-Ying Ma(马凤英), Xi Wang(王茜), Yuan-Zhuang Bu(卜远壮), Yong-Zhi Tian(田勇志), Yanli Du(杜艳丽), Qiao-Xia Gong(弓巧侠), Ceyun Zhuang(庄策云), Jinhai Li(李金海), and Lei Li(李磊)
Chin. Phys. B, 2021, 30 (**4**): 044202. DOI: 10.1088/1674-1056/abd2aa

Beam steering characteristics in high-power quantum-cascade lasers emitting at ~4.6 μm

Yong-Qiang Sun(孙永强), Jin-Chuan Zhang(张锦川), Feng-Min Cheng(程凤敏), Chao Ning(宁超), Ning Zhuo(卓宁), Shen-Qiang Zhai(翟慎强), Feng-Qi Liu(刘峰奇), Jun-Qi Liu(刘俊岐), Shu-Man Liu(刘舒曼), and Zhan-Guo Wang(王占国)
Chin. Phys. B, 2021, 30 (**3**): 034211. DOI: 10.1088/1674-1056/abd6fe

---

Real time high accuracy phase contrast imaging with parallel acquisition speckle tracking*

Zhe Hu(胡哲)[1,2], Wen-Qiang Hua(滑文强)[1,3], and Jie Wang(王劼)[1,3,†]

[1] *Shanghai Institute of Applied Physics, Chinese Academy of Sciences, Shanghai* 201800, *China*
[2] *University of Chinese Academy of Sciences, Beijing* 100049, *China*
[3] *SSRF, Shanghai Advanced Research Institute, Chinese Academy of Sciences, Shanghai* 201204, *China*

(Received 21 January 2021; revised manuscript received 9 March 2021; accepted manuscript online 12 March 2021)

X-ray speckle tracking based methods can provide results with best reported angular accuracy up to 2 nrad. However, duo to the multi-frame requirement for phase retrieval and the possible instability of the x-ray beam, mechanical and background vibration, the actual accuracy will inevitably be degraded by these time-dependent fluctuations. Therefore, not only spatial position, but also temporal features of the speckle patterns need to be considered in order to maintain the superiority of the speckle-based methods. In this paper, we propose a parallel acquisition method with advantages of real time and high accuracy, which has potential applicability to dynamic samples imaging as well as on-line beam monitoring. Through simulations, we demonstrate that the proposed method can reduce the phase error caused by the fluctuations to 1% at most compared with current speckle tracking methods. Meanwhile, it can keep the accuracy deterioration within 0.03 nrad, making the high theoretical accuracy a reality. Also, we find that waveforms of the incident beam have a little impact on the phase retrieved and will not influence the actual accuracy, which relaxes the requirements for speckle-based experiments.

Keywords: phase contrast imaging, near field speckle, grating splitter

PACS: 42.30.–d, 42.30.Ms, 42.30.Rx **DOI:** 10.1088/1674-1056/abee08

1. Introduction

While conventional x-ray imaging is based on the local attenuation of a photon beam,[1,2] phase contrast imaging detects the real part of complex refraction index of a sample.[3–5] In x-ray field, the real part is several orders larger in magnitude than the imaginary part, leading to a higher sensitivity to small density differences, which also can significantly increase the contrast in imaging.[3]

Currently, various methods such as coherent diffraction imaging,[6] transport of intensity equation,[7] Hartmann wavefront sensing,[8] and propagation-based (in-line) methods,[9] grating-based method,[10,11] as well as Talbot grating interferometry[12] are available to quantitatively measure the phase of a beam or sample. One of the latest additions to the group of differential phase-contrast methods is the x-ray near field speckle based technique.[13–15] It has drawn significant attention due to its simple and flexible experimental arrangement and high angular accuracy, amongst others. The best reported angular accuracy in the literature is 2 nrad.[15]

In general, two or more frames of speckle patterns are the prerequisite of phase retrieval processing. Therefore, so far, sequential patterns measurements are applied, for instance, patterns of sample-in and -out or scanning of the speckle mask are acquired. Current speckle tracking (CST) method treats speckle patterns as functions of spatial position only.[13–15] However, no matter in single-shot way or scanning way, the requirements for moving objects, detectors, or speckle masks raise strong challenges on the external aspects such as stability of the beam, machine, etc.[16] In the synchrotron radiation, the vibration of the light source, oscillation of the vacuum pump and water cooling unit will frequently change the incident beam, leading to changes of the beam size, position, and wavefront over time. These will introduce errors that are unpredictable and difficult to eliminate in phase retrieval if the spatial position of speckle patterns is considered only. There are many ways to improve the accuracy in imaging, such as using generative adversarial network to remove background noise,[17] or using filters to remove electric noise and roundoff error.[18] However, it is difficult to find a certain rule to eliminate errors mentioned above due to the time-varying beam size and position. Usually, fast acquisition or parallel acquisition methods can reduce these kinds of errors. Yet the former one is limited by the speed of mechanical motion and acquisition time of images. So, a parallel acquisition speckle tracking (PAST) method is proposed in this paper. It combines near field speckle and property of grating splitter[19] to collect sample and reference images simultaneously. In this case, errors introduced by external fluctuations will be recorded in all images and can be eliminated naturally by our algorithm, leading to more robust and accurate results. It should be mentioned that the method proposed here is somehow similar to

*Project supported by the National Natural Science Foundation of China (Grant Nos. 11675253 and 11505278).
†Corresponding author. E-mail: wangjie@zjlab.org.cn
© 2021 Chinese Physical Society and IOP Publishing Ltd

the previous method described in Ref. [14], which uses two detectors along the optical path to quantitatively analyze x-ray pulsed wavefronts. The differences lie in the following two aspects. Firstly, the proposed method not only can work like the method in Ref. [14] to perform on-line beam phase sensing, but also can recover the phase of the sample alone, depending on the relative position of the two detectors. Secondly, combining the property of grating and Fourier based solver[16] for propagation-based method, the resolution can be a pixel size rather than the average speckle grain size.

2. Method

To combine near field speckle with grating splitter, working principle of these two methods needs to be clarified here. Firstly, the size and shape of the near field speckle grains will not change within a critical distance defined as $z_c = D^2/\lambda$ (D is the transversal coherence size and λ is the wavelength).[13] This property allows the near field speckle to be used as a wavefront marker for phase retrieval. Any phase object introduced into the beam path will distort the wavefront and modulate the speckle pattern. The differential phase shift of the x-ray wavefront can be obtained by tracking modulations of the speckle pattern using the digital imaging correlation (DIC) algorithm[20] or geometric flow method.[16] The relative displacement of every pixel $P(x_0, y_0)$ in the unitary base (x, y) is obtained (Fig. 1(a)) as

$$\begin{aligned} x_0'(t_1) &= x_0(t_2) + \varepsilon(\Delta t, \delta t, x_0, y_0), \\ y_0'(t_1) &= y_0(t_2) + \tau(\Delta t, \delta t, x_0, y_0), \end{aligned} \tag{1}$$

where $\Delta t = t_1 - t_2$ is the time interval between the collection of two images, δt is exposure time, and $\varepsilon(\Delta t, \delta t, x_0, y_0)$, $\tau(\Delta t, \delta t, x_0, y_0)$ reflect the time-varying displacement of the target subset from the reference subset centered on $P(x_0, y_0)$. For methods with angular accuracy of nanoradians, the extra displacement contained in ε and τ will degrade the imaging quality and accuracy strongly. So, temporal features need to be eliminated to get more accurate results.

The relationship between the speckle displacement, angular offset Θ_m of the beam and the phase differential can be described as below:[13]

$$\Theta_m \cong \frac{v_{x,y}}{\Delta l} = \frac{\lambda}{2\pi} \frac{\partial \Phi(x,y)}{\partial m}, \quad (m = x, y), \tag{2}$$

where Δl is the distance of sample to detector and $\Phi(x, y)$ is the phase function of the sample. Once displacement of every pixel is obtained, we can use the partial derivatives in two directions to recover the phase. The theoretic accuracy[13] can be described as $\sigma = s \times \delta_a/\Delta l$, where δ_a is the pixel accuracy of the cross correlation function, s represents pixel size for single shot methods or scanning step size for scanning-based technique.

Secondly, as shown in Fig. 1(b), when a grating splitter is inserted into a beam path, a series of diffracted light will be produced. According to Ref. [19], the intensity distribution, coherence, and wavefront of the first-order diffracted beam of a grating preserves the properties of the incident beam. This needs to be achieved in the far-field corresponding to the grating to separate the diffracted light. The distance can be described by $z_p = p^2/\lambda$, where p is the period of the grating. The influence of the grating imperfection cannot be neglected for its direct participation in optical process. $\Delta n/n$ (n is the linear density of a grating) is used to describe the density variation of the grating, which influences the diffraction angle. Consider the commercial x-ray grating whose $\Delta n/n$ can be 10^{-5}, and let $\lambda = 0.1$ nm, $n = 500$/mm. According to the diffraction formula, $\sin\theta - \sin\theta_0 = n\lambda$ (θ is the diffraction angle and θ_0 is the incident angle), the corresponding diffraction angle deviation caused by grating imperfection is 0.5 nrad, which can be basically neglected.

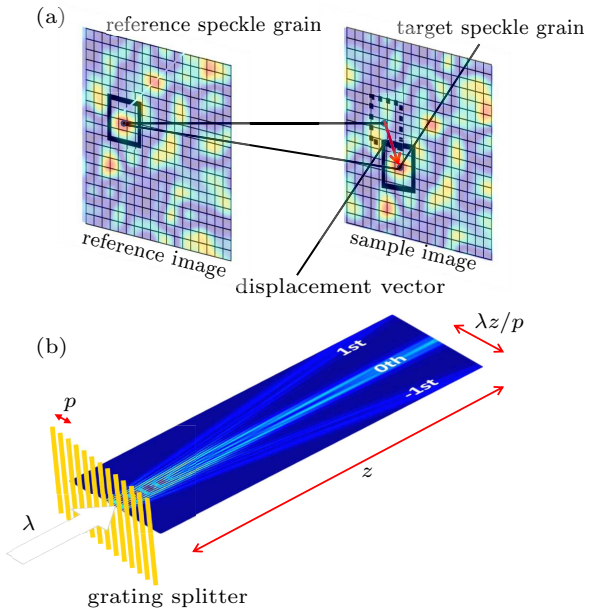


Fig. 1. (a) Principle of near-field speckle tracking. The displacement of every speckle grain is tracked from two images. The red arrow indicates displacement of the subset. (b) Demonstration of diffraction of grating splitter.

Comparing z_c with z_p makes requests for experiments that the transverse coherent length D should be larger in magnitude than the grating period p if we combine near field speckle with the property of grating splitter. The incident beam first passes through a speckle mask to create speckle. Then, a grating splitter will split it into a series of diffraction beams. Samples will be put into the zeroth order beam. Due to the property of the grating splitter,[19] we can record the zeroth and first order beams as reference and sample image, respectively. In this way, errors caused by time-varying fluctuations will be recorded in both images. These errors can be naturally removed because they contribute the same shift of speckle grains

in each image and can be recognized by algorithms

$$x_0'(t)+e_1(\delta t,x_0,y_0)=x_0(t)+e_1(\delta t,x_0,y_0)+\varepsilon(x_0,y_0),$$
$$y_0'(t)+e_2(\delta t,x_0,y_0)=y_0(t)+e_2(\delta t,x_0,y_0)+\tau(x_0,y_0), \quad (3)$$

where $e_1(\delta t,x_0,y_0)$ and $e_2(\delta t,x_0,y_0)$ are speckle displacement errors introduced by time-varying fluctuations during the exposure time. Equations (3) and (1) are essentially the same except that ε and τ no longer change with time, which means the proposed method eliminates errors related to temporal features of the speckle patterns. In this case, the values of ε and τ are only related to the phase of samples, leading to a great improvement to the accuracy and robustness of the phase retrieval results.

3. Simulations

Simulations of two frameworks shown in Figs. 2(a) and 2(b) were performed to test the proposed method. Firstly, two sets of speckle patterns about a preset sample were obtained using the two configurations. The same algorithm was used to process the data to recover phases. Then, the results obtained were compared to the preset sample to get residual error maps and root mean square error (RMSE), and RMSE is used to quantify the accuracy of phase retrieved.

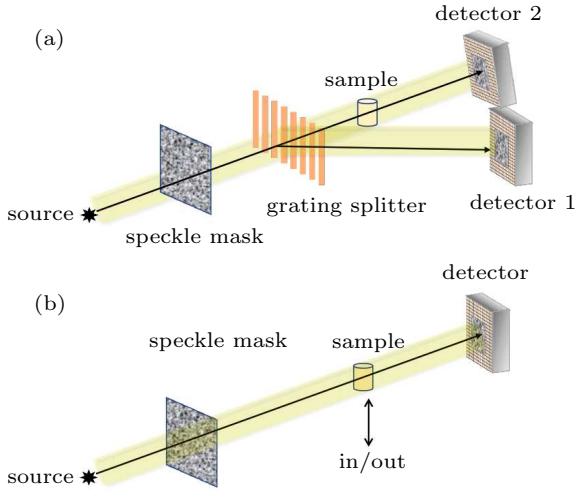


Fig. 2. Experiment configurations of (a) the proposed method and (b) CST.

In these simulations, the preset sample (Fig. 3(a)) and the incident wavefront (Fig. 3(b)) were defined on a 256×256 grid with 1 μm×1 μm pixel size. The wavelength of hard x-ray is 0.1 nm. Angular spectrum numerical propagation is used to produce speckle patterns. The distance between the grating splitter, sample, and detectors are set to be 0.1 m and 1 m, respectively. To simulate the time-varying external fluctuations, we add small random disturbance functions described as $\Phi(x,y)=A\exp\left(-\frac{(x-a)^2}{2\times10^{-8}}-\frac{(y-b)^2}{2\times10^{-8}}\right)$ to each incident wavefront to simulate the time-varying incident wavefront. Here A is the amplitude, the value range of a and b is $[-100\times10^{-6}, 100\times10^{-6}]$ m. Obviously, if $A=0$, i.e., the absence of the fluctuations, the residual error corresponds to the 'intrinsic error' limited by the theoretic accuracy σ, which is invariant because of the uniqueness of the result obtained by the same algorithm. The speckle patterns processed by the algorithm are the superimposition of ten patterns obtained from ten different incident wavefronts, just like the detector collects the time-integrated intensity information.

First of all, we set $A=1$ to see the performance of the two methods. Two retrieved phases corresponding to CST and PAST with RMSE values of 0.0672 and 0.0005 are recovered, and the residual error maps are shown in Figs. 3(c) and 3(d). We can see that the proposed method performs better in the presence of external fluctuations.

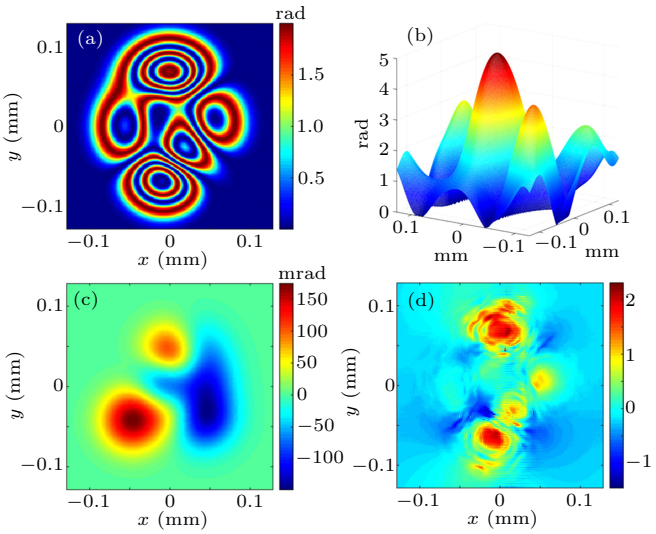


Fig. 3. (a) The preset sample. (b) Incident wavefront. (c)–(d) Residual error maps of CST and PAST, respectively.

Then, we set those external disturbance functions unchanged except their amplitudes increase from 0 to 1 to see how the phase errors will change. By repeating the procedure mentioned above, we get a series of recovered phases. And the RMSE values are summarized in Fig. 4(a).

We can conclude from Fig. 4(a) that when the amplitude of fluctuations increases linearly, the RMSE of CST increases almost linearly as well. This means the effects of fluctuations at different times on the CST are linearly superimposed. Meanwhile, the errors of the proposed method remain almost unchanged in Fig. 4(a), meaning the significant error reduction capability of the proposed method. We compare the two sets of RMSE values and find that PAST can reduce errors to about 1% at most compared with CST. It is reasonable to predict that this gap will continue to grow as A increases.

We also explore the influence of the incident waveforms under PAST. Different incident wavefronts of randomly distributed (Fig. 3(b)), planar, spherical, and Gaussian are simulated. Figure 4(b) presents the RMSE values obtained as a function A for four wavefronts. It can be seen clearly that the plane wave has the optimal performance under the disturbed environment comparing to the others. Nonetheless, the quality of phase recovered does not change significantly within

a broad range for all kinds of wavefronts, which implies the requirements for speckle-based experiments on the incident wavefront can be relaxed.

We introduce σ_e to describe the accuracy deterioration caused by the coupling results of the time-varying fluctuations during the time interval between the collection of two images and the exposure time. And σ_e is defined as the root mean square of the difference of the residual error maps when $A \neq 0$ and $A = 0$. Here, we treat the residual error map when $A = 0$ as the true value because of its invariance. The σ_e of the two methods under different waveforms are plotted in Figs. 4(c) and 4(d) as a function of A. It can be seen clearly that the lines representing different waveforms are overlapped for both methods, indicating that the waveforms do not affect the accuracy of the experiments. On the contrary, the increase of the magnitude of A affects the accuracy linearly, which means the larger the coupling result of fluctuations is, the worse the experimental accuracy is. This linear characteristic, in turn, illustrates the rationality of taking the residual error map when $A = 0$ as the true value. We can see that the maximum σ_e of the proposed method is 0.03 nrad, while more than 60 nrad for that of CST, meaning the high theoretical accuracy can only be realized by the proposed method.

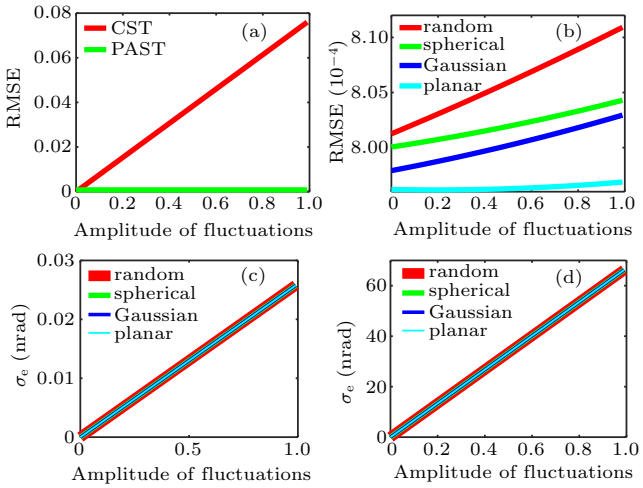


Fig. 4. (a) The RMSE values of the two methods plotted as a function of the amplitude of time-varying fluctuations. (b) Influence of four different incident wavefronts on PAST. (c)–(d) Angular accuracy deterioration σ_e of PAST and CST as a function of amplitude of time-varying fluctuations, respectively.

In conclusion, we have proved that the proposed method can provide robust and much more accurate results than the conventional speckle tracking method in the presence of external fluctuations.

4. Experiments

Due to the lack of grating for x-ray in our laboratory currently,[21] we carried out experiments with visible light. The experimental layout of the proposed method is shown in Fig. 5. The illumination system is consisted of a He–Ne laser beam with central wave length of 632.8 nm, a collector lens, a circular aperture, and a condenser lens. The images are captured by CCD cameras (Hamamatsu C11440-36U, 19201200, pixel size $s_{pix} = 5.86$ μm, 125 fps). Calibrated laser beam passes the frosted glass with grain size of 15 μm to generate speckle pattern. A grating with period of 9 μm is used to produce diffraction beam. We used a lens with focus length of 100 mm as the sample. The distance between the grating splitter and sample is 20 cm. And the sample to detector distance is 1 cm. The acquisition time of each image is 1 ms.

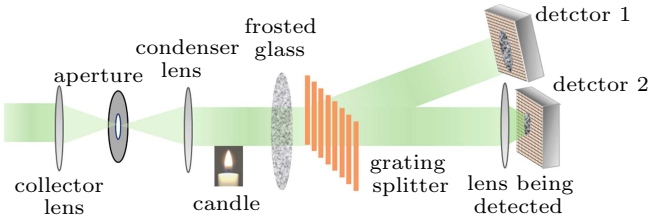


Fig. 5. Experimental layout of PAST with visible light.

In the first step, we checked the phase retrieval capability of the proposed method. Two sets of data corresponding to the two methods were obtained and processed to get two recovered phases (Figs. 6(a) and 6(b)). Then, a residual error map (Fig. 6(c)) was obtained by subtract the two phase maps. The corresponding RMSE value is 0.11. So, the phase retrieval ability of the proposed method is validated. The spatial resolution of PAST and CST is 5.86 μm, the theoretical angular accuracy of the two methods is the same, which is 30 μrad according to the equation mentioned above.

Then, we examined if the proposed method can reduce errors under a disturbed environment comparing to CST. To simulate the instability of the x-ray beam, machinery vibration in x-ray field, we used the air fluctuations caused by the heat of a lit candle to change the incident wavefront. We noticed during the experiments that when the acquisition time is long, the influence of external fluctuations to images is smoothed out, despite there still exist errors. However, at the acquisition time of 1 ms, the influences become visible even to a naked eye. We repeated the procedural mentioned above and set the result of CST in the first step as a standard. By comparing it with two newly retrieved phases, we got two residual error maps corresponding to PAST and CST (Figs. 6(d) and 6(e)). And the RMSE values are 0.37 and 13.81, which indicates the phase recovered by the proposed is almost unaffected by time-varying fluctuations while big error appears in the result of CST. We repeated the experiments 20 times and got the standard deviation of RMSE values of the proposed method and CST, 0.089 and 2.16, which implies the good stability and accuracy of the results recovered by PAST despite the presence of strong external fluctuations. Meanwhile we can use the root mean square of the subtraction of Figs. 6(d) and 6(e) to get the accuracy deterioration σ_e of CST. The result is 13.01 rad, which means the angular accuracy of CST is completely ruined by the external fluctuations.

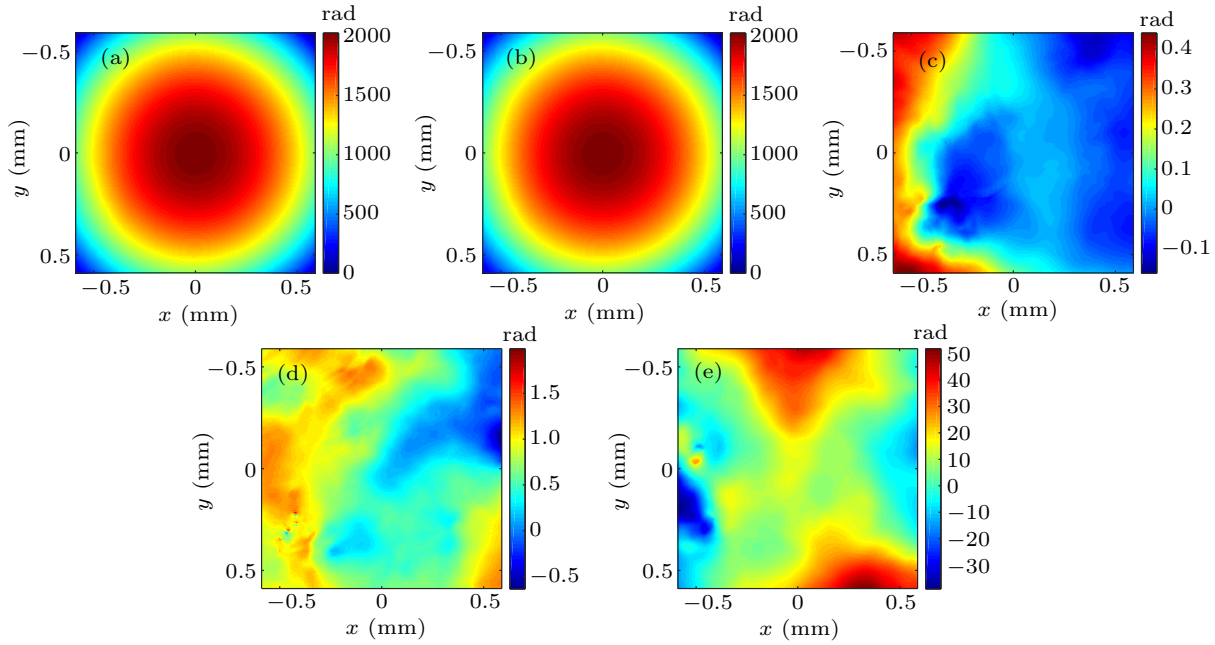


Fig. 6. (a)–(b) Phase recovered by PAST and CST. (c) Residual error map. (d)–(e) Residual error maps corresponding to PAST and CST under a disturbed environment.

5. Conclusion

In summary, we have demonstrated a real-time, high accuracy method for speckle-based phase contrast imaging. Through simulations and experiments, we show that this method can reduce errors introduced by time dependent fluctuations to 1% when compared with current speckle tracking method. Meanwhile, it can preserve high theoretic accuracy, which implies a huge increase of fidelity and robustness to the experiments. Meanwhile, it has two other major advantages. First, due to the simultaneous collection of reference and sample images, it can recover the phase functions at any instant, which may be useful for on-line beam monitoring of x-ray free electron laser. Second, by combining with the FFT based solver,[14] our method can provide a real time rapid imaging, which is suitable for imaging living patients and dynamic samples. Nevertheless, when used in x-ray field, this method requires grating with high linear density, which poses high requirements on grating processing technology. In future work, we will try to change wavefront of the incident beam in some ways in x-ray field and collect two first order diffraction beams to monitor it. It can be used in fields such as super resolution of phase retrieval.[22] We will demonstrate it in the future investigation.

Acknowledgement

Authors wish to thank Dr. Feixiang Wang and Dr. Haipeng Zhang for helpful discussions.

References

[1] Diemoz P C, Coan P, Glaser C and Bravin A 2010 *Opt. Express* **18** 3494
[2] Colin N 2018 *J. Synchrotron Radiat.* **25** 1490
[3] Fitzgerald R 2000 *Phys. Today.* **53** 23
[4] Mao H X, Panna A, Gomella A A, Bennett E E, Znati S, Chen L and Wen H 2016 *Nat. Phys.* **12** 830
[5] Lin Y Z, Huang K Y and Luo Y 2018 *Opt. Lett.* **43** 2973
[6] Pan X C, Veetil S P, Liu C, Lin Q and Zhu J Q 2013 *Chin. Opt. Lett.* **11** 39
[7] Zuo C, Chen Q and Asundi A 2014 *Opt. Express* **22** 9220
[8] Rais M, Morel J M, Thiebaut C, Delvit J M and Facciolo G 2016 *Appl. Opt.* **55** 7836
[9] Cloetens P, Ludwig W, Baruchel J, Dyck D V, Landuyt J V, Guigay J P and Schlenker M 1999 *Appl. Phys. Lett.* **75** 2912
[10] Faiz W, Li j, Gao K, Wu Z, Lei Y H, Huang J H and Zhu P P 2020 *Chin. Phys. B* **29** 014301
[11] Faiz W, Bao Y, Gao K, Wu Z, Wei C X, Zan G B, Zhu P P and Tian Y C 2017 *Chin. Phys. B* **26** 040602
[12] Momose A, Yashiro W, Maikusa H and Takeda Y 2009 *Opt. Express* **17** 12540
[13] Bérujon S, Ziegler E, Cerbino R and Peverini L 2012 *Phys. Rev. Lett.* **108** 158102
[14] Bérujon S, Ziegler E and Cloetens P 2015 *J. Synchrotron Rad.* **22** 886
[15] Kashyap Y, Wang H C and Sawhney K 2016 *Rev. Sci. Instrum.* **87** 2562
[16] Paganin D M, Labriet H, Brun E and Bérujon S 2018 *Phys. Rev. A.* **98** 053813
[17] Wolterink J M, Leiner T, Viergever M A and Išgum I 2017 *IEEE Transactions on Medical Imaging* **36** 2536
[18] Diwakar M and Kumar M 2018 *Biomed. Signal Process. Control* **42** 73
[19] Hua W Q, Zhou G Z, Hu Z, Yang S M, Liao K L, Zhou P, Dong X H, Wang Y Z, Bian F G and Wang J 2019 *J. Synchrotron Radiat.* **26** 619
[20] Pan B, Qian K, Xie H and Asundi A 2009 *Measurement Science & Technology* **20** 062001
[21] Makita M, Karvinen P, Guzenko V A, Kujala N, Vagovic P and David C 2017 *Microelectronic Engineering* **176** 75
[22] Zhang H, Jiang S W, Liao J, Deng J J, Liu J, Zhang Y B and Zheng G A 2019 *Opt. Express* **27** 7498